

An atlas of spectra of B6-A2 hypergiants and supergiants from 4800 to 6700 Å^{*}

E. L. Chentsov^{1,2}, S. V. Ermakov^{1,2}, V. G. Klochkova^{1,2}, V. E. Panchuk^{1,2}, K. S. Bjorkman³, and A. S. Miroshnichenko^{3,4}

¹ Special Astrophysical Observatory of the Russian Academy of Sciences, Karachai-Circassian Republic, Nizhnij Arkhyz, 369167, Russia

² Isaac Newton Institute of Chile, SAO Branch

³ Ritter Observatory, Dept. of Physics & Astronomy, University of Toledo, Toledo, OH 43606-3390, USA

⁴ Central Astronomical Observatory of the Russian Academy of Sciences at Pulkovo, 196140, Saint-Petersburg, Russia

received date, accepted date

Abstract. We present an atlas of spectra of 5 emission-line stars: the low luminosity LBVs HD 168625 and HD 160529, white hypergiants – LBV candidates HD 168607 and AS 314, and supergiant HD 183143. The spectra were obtained with 2 échelle spectrometers at the 6-m telescope of the Russian Academy of Sciences at a range from 4800 to 6700 Å and a resolution of 0.4 Å. We identified 380 spectral lines and diffuse interstellar bands. Spectral features of the objects are described.

Key words. Stars: emission-line Stars:individual HD 160529, HD 168607, HD 168625, HD 183143, AS 314
Techniques: spectroscopic

1. Introduction

This paper presents a comparative description of optical spectra of several white hypergiants and supergiants, a result of a study of stars with dense slow winds and pseudophotospheres (in particular, LBVs). As the luminosity of LBVs decreases, the interval of the effective temperature variations becomes narrower, so that its lower boundary remains the same (Humphreys & Davidson 1994). In the least luminous LBVs, this interval is bound between 12000–13000 and 7500–8000 K (latest B-subtypes and earliest A-subtypes, respectively). Such objects are very rare: only 2 of them have been found in the Milky Way so far (van Genderen 2001). Both of these objects are presented here (HD 168625, B6Ia⁺, and HD 160529, B8–A3 Ia⁺), along with the 2 LBV candidates (HD 168607, B9 Ia⁺, and AS 314, Ia) and the supergiant HD 183143 (B7 Ia). A detailed comparison of their spectra with each other as well as with those of other objects may help in a search for new spectroscopic criteria to distinguish LBVs from quasi-stationary hypergiants, on one hand, and from lower-mass supergiants at the post-AGB stage, on the other.

Send offprint requests to: E. L. Chentsov, e-mail: echen@sao.ru

^{*} The whole atlas is only available in electronic form at the CDS via anonymous ftp ([cdsarc.u-strasbg.fr](ftp://cdsarc.u-strasbg.fr) or 130.79.128.5) or by web access to <http://cdsweb.u-strasbg.fr/A+A.htm>

In this connection, as well as on its own, one of the spectroscopic features of the stellar wind is particularly interesting. The broad P Cyg-type absorptions can have moving local depressions, which appear initially at the red edge of the absorption component and later move to the blue edge (also known as “discrete absorption components”, DACs). This effect was first discovered in the only LBV of the northern sky, P Cyg (Markova 1986). Since then, it has been described in hypergiants earlier than B2 (Fullerton, Gies, & Bolton 1992, Rivinius et al. 1997) and later than B9 (Chentsov 1995, Kaufer et al. 1996). We believe that HD 168625 and HD 183143 are objects which may fill the gap in the late B-type stars.

In Table 1 we present our estimates of the spectral types and absolute visual magnitudes of the studied objects, their optical brightnesses, galactic coordinates, and dates of the observations. HD 183143 is located between the local spiral arm of the Milky Way and the closest internal arm of Sagittarius–Carina, while the other objects belong to the latter.

2. Observations and data reduction

The spectra were obtained at the 6-m telescope of the Special Astrophysical Observatory (SAO) of the Russian Academy of Sciences using 2 échelle-spectrometers, PFES (Panchuk et al. 1998) and LYNX (Panchuk et al. 1999).

Table 1. Main parameters of stars studied

Star	Sp	M_v	V	l	b	Date*
HD168625	B5.7	-8.5	8.4	15	-1.0	19.06.98(P) 4.06.99(L) 24.06.00(L)
HD183143	B7.8	-7.7	6.9	53	0.6	5.06.99(L) 7.06.01(P)
HD168607	B9.4	-8.8	8.3	15	-1.0	19.06.98(P) 24.06.00(L) 4.06.01(P)
AS 314	A0	-7.5	9.8	19	-3.7	30.06.99(L) 5.07.00(P) 4.06.01(P)
HD160529	A2	-8.9	6.6	356	-1.7	4.06.01(P)

* - P- PFES; L - Lynx

PFES is mounted in the prime focus cage and is equipped with a CCD detector having 1160×1040 pixels, $16 \times 16 \mu\text{m}$ size each. It provides a spectral resolving power of $R \sim 15000$ in the range 4500–7930 Å. LYNX is mounted in a Nasmyth focus and, with the same CCD, provides a $R \sim 25000$ in the range 4725–6325 Å.

Parts of the spectra included in the atlas are limited to the range between 4800 and 6700 Å due to a significant sensitivity reduction of the CCD shortward of this range and effects of the atmospheric and interstellar extinction, and to the wide telluric bands affecting the spectra longward of it. The signal-to-noise ratio in the chosen spectral range for all the spectra shown in this atlas is higher than 100. Combining with the spectral resolving power, it allowed us not only to detect rather weak lines but also to study their profiles.

The 2D spectra were reduced (applying standard procedures of bias subtraction, scattered light and cosmic ray trace removal, and order extraction) using the task ECHELLE under MIDAS (version 1998). Further measurements (photometric and positional) in the 1D spectra were made in the DECH20 package (Galazutdinov 1992). In particular, positions of the spectral lines were measured by matching the original and mirrored profiles. Instrumental corrections for the measured wavelengths were derived using telluric lines of oxygen and water. Special care was taken deriving these corrections in the spectra obtained with PFES, which is mechanically and thermally less stable than LYNX. The residual systematic corrections, estimated using interstellar lines of Na I and K I, do not exceed 2 km s^{-1} . The laboratory wavelengths, used to measure radial velocities (RV), were taken from tables of Striganov & Odintsova (1982), Johansson (1978), and Chentsov, Musaev, & Galazutdinov (1996). The diffuse interstellar bands (DIBs), very strong in the spectra of our objects, significantly differ from each other in both strength and depth. The broadest of them (e.g., at 4820, 4880, and 4970 Å) are poorly seen in échelle spectra, because they occupy most of the corresponding order width. On the other hand, there are many DIBs (e.g., at 5780,

5797, and 5850 Å) which have widths comparable to those of stellar absorption lines. We measured RVs of only the latter DIBs using an atlas of Galazutdinov et al. (2000).

3. Atlas and list of identified spectral lines

The spectra of all 5 stars in the range 4800–6700 Å are presented in the form of intensities, normalized to the underlying continuum, versus laboratory wavelengths. The atlas is divided into sections 120 Å in width. As an example, the fragment within the spectral region λ 4990–5110 Å is shown in Fig. 1. In every section, the objects are shown in the same order as in Table 1, i.e. with the effective temperature decreasing from top to bottom.

As seen from Table 1, we used several spectra, obtained at different time and with different spectrometers, for 4 out of 5 objects. Fig. 1 shows averaged spectra of these objects. The RVs and profiles of some lines vary with time. This is why for the atlas we have chosen the spectra with minimum differences in the line profiles with respect to each other in order to show characteristic profiles of these lines.

The list of 380 identified stellar, circumstellar and interstellar lines and DIBs is presented in Table 3. Any line found in the spectrum of an object is listed in the corresponding column with the residual central intensity normalized to the continuum (r). In the case of a blend, the value is listed for the stronger component. For example, it is N II (Mult. 19) 5001.3 Å in HD 183143 and Fe II 5001.9 Å in HD 168607. For the P Cyg-type profiles we list extremal values of both the absorption and emission components. The weakest of the detected lines have $r = 1 \pm 0.01$.

Table 2. Average heliocentric radial velocities \overline{RV}

Name(HD)	168625	183143	168607	AS314	160529
Data	4.06.99	5.06.99	18.06.95	5.07.00	4.06.01
	Emis. lin/comp ($r \rightarrow 1$)				
	10 -60				
	Abs. lin/comp				
HeI, SII, ... ($r \rightarrow 1$)	17	11	11	-43	-28
FeII high ex.			0	-40	-30
SiII (2)	12	13	-2	-52	-26
FeII low ex. ($r \rightarrow 1$)			-15	-102	-14 -60 -104
FeII (42)	12	13	-14 -75 -120	-106	-75 -104
H α	-35 -105	-47	-75 -120	-112	-105
	Abs. I.S.				
NaI (1)	1	0		-5	-14
DIB	10	-3	8	-7	-6

In the spectra of HD 168625 and HD 183143 the lines were identified traditionally – by the RVs and relative intensities. However, we used the latter criterion within the spectrum of an object as well as while comparing spectra of different objects. We mean not only strengthening or weakening of absorption lines from the hotter to the cooler stars, but also the transformation of absorptions into emissions or appearance of emission components in absorption lines. There are about 20 % emission lines in the spectra of HD 168607 and AS 314. In the spectrum of HD 160529 emission lines are found more rarely, but most of the absorption lines are split into several components. The specific shapes of the line profiles are indicators of the atmospheric expansion and the presence of a RV gradient. They can also be used as additional criteria for line identification.

Weak lines are dominant in the spectra of late-B subtypes. In our list the fraction of absorptions with $r \gtrsim 0.9$ is about 90 % for HD 168625, HD 183143 and HD 168607, 85 % for AS 314, and 75 % for HD 160529. In the spectrum of the hottest of our stars, HD 168625, we found lines of H I, He I, C II, N II, O I, Ne I, Al III, Si II, Si II, S II, Fe II, and Fe III. In the spectrum of the coolest star, HD 160529, some of these lines are also seen, but lines of N I, Na I, Mg I, Mg II, Al II, Sc II, Ti II, Cr II, Mn II, Fe I, and Ba II are present instead of C II, N II, Al III, Si III, and Fe III.

4. Spectroscopic features of the objects

As mentioned above, all the objects are more or less spectroscopically variable: the line profile shapes and RVs change differently with time. We group most of the lines (or their components), which either have a constant RV or it gradually changes along with the line intensity. The mean RVs for some such groups are collected in Table 2, where each object is represented by one spectrum whose observing date is listed. A note $r \rightarrow 1$ represents the limit, which the RV of an absorption line or an absorption component of the P Cyg-type profile is approaching with the increasing r (or decreasing depth). In other words, it corresponds to the RVs of the weakest absorption lines or components. Below we discuss typical features of the spectrum of each object.

4.1. HD 168607

HD 168607 has the most interesting and best studied spectrum. It has been described by Chentsov & Luud (1989) and Chentsov & Musaev (1996). One can nicely see its features comparing the spectra of HD 168607 and HD 183143 in Fig. 1. Differences in the intensity and profile shape are small not only in the He I and light ion lines, but also in the Fe II absorptions with low level excitation potentials of more than 10 eV. At the same time, the latter and the strong absorptions of Si II (2) in the spectrum of HD 168607 are blueshifted by $\sim 12 \text{ km s}^{-1}$ with respect to the former (see Table 2 and Fig. 2a). Since the Fe II and Si II lines are formed in the atmosphere above those

of the light elements, this differential shift can be interpreted as evidence that corresponding atmospheric layers are expanding.

Relations between VRs and r for HD 168607 are shown in Fig. 2a. Lagre filled circles, which represent individual absorption lines or absorption components of P Cyg profiles, form several horizontal sequences. The upper sequence represents pure (photospheric) absorption lines of He I, C II, etc. In the range $0.75 \leq r \leq 0.98$, they give a mean $\text{RV} = 11 \text{ km s}^{-1}$ with a scatter due to measurement errors only. As we mentioned above, the lowest RV have the strong Si II 6347 Å line and the weak Fe II high excitation lines.

The other horizontal sequences represent discrete components, in which absorption parts of P Cyg-type profiles of the H α , H β and Fe II lines with low excitation potentials of the low levels ($\sim 3 \text{ eV}$) are split. These are strictly horizontal: the RVs are independent of r . The upper of these sequences ($\text{RV} = -14 \text{ km s}^{-1}$) relates to the deepest wind components of the Fe II lines, which is not observed in the Balmer lines due to a strong emission at this RV. The other two sequences ($\text{RV} = -75$ and -120 km s^{-1}) include weak components of the Fe II lines and strong components of the Balmer lines. This effect is additionally illustrated in Fig. 3, where the profiles of 2 lines of Fe II with different intensities are compared.

The described picture is not characteristic of hot luminous stars with strong winds. For example, a gradual decrease of VR with increasing r is noticed in the spectrum of P Cyg, a prototype of such stars (de Groot 1969). The same effect is observed in AS 314 (see Sect. 4.4 and Fig. 2b). Perhaps, in the case of HD 168607 we deal with an asymmetric wind or multiple detached envelopes with different expansion velocities and small radial velocity gradients. Thus, a spectroscopic monitoring of HD 168607 is highly desirable.

It is also shown in Fig. 3 how the profiles of different lines are changing with time. While a photospheric absorption of He I and emission parts of the Fe II line profiles changed a little, wind absorption components of the latter redistributed completely. In our data, they can assume any position between -10 and -140 km s^{-1} .

As the absorption components of the lines with P Cyg profiles become weaker, the RVs of their emission peaks approach the mean value for the symmetric stationary emissions of Fe II ($z^4\text{D}-c^4\text{D}$) (see Fig. 3). The latter are probably formed in extended spherically-symmetric envelopes. The corresponding mean RV, 10 km s^{-1} , is listed in the first line of Table 3 and is adopted as the RV of the centre of the star's mass.

4.2. HD 168625

This star is considered an LBV because of its circumstellar envelope, gaseous and dusty components of which have been described in detail by Hutsemekers et al. (1994), Nota et al. (1996), and Robberto & Herbst (1998).

However, neither photometry (van Genderen et al. 1992) nor spectroscopy (Chentsov & Luud 1989, Nota et al. 1996) revealed any of the LBV features in this star. As seen in Fig. 1 and Table 3, the spectrum of HD 168625 is very similar to that of HD 183143. Differences, which are illustrated by blends of He I–Fe II at 4922/24 and 5015/18 Å, reflect only the temperature difference. In our spectral region significant profile variations are seen only in the hydrogen lines. Their RVs also vary significantly (by tens km s^{-1}) with time and from line to line (Balmer progression). For the other lines amplitudes of the temporal variations and differential shifts are limited to a few km s^{-1} . The absorptions of He I, C II, N II, Al III, Si III, S II, and Fe III, whose intensity maxima are reached in B2–5 spectral types, have RVs very close to each other and are grouped together (hereafter, the He I lines and others). The weakest of them are formed in the deepest photospheric layers of HD 168625 reachable with our spectral resolving power. Table 2 lists the RV of these lines obtained on 1999 June 4 ($+17 \text{ km s}^{-1}$), while the RVs measured in our other spectra of the object vary between $+8$ and $+12 \text{ km s}^{-1}$. The absorptions of Si III(2) and Fe II(42) are formed higher in the atmosphere and are usually shifted bluewards with respect to the He I lines and others. Apparently, the RV variations are due to atmospheric pulsations, while the line differential shifts are due to the atmospheric expansion.

The angular distance between HD 168625 and HD 168607 is only 1 minute of arc, and both stars are located in the vicinity of the M17 nebula. Hence, their close position is hardly occasional. Nevertheless, there are suggestions that the distance towards HD 168625 is much smaller (Robberto & Herbst 1998) or larger (Hutsemekers et al. 1994) than that towards HD 168607. The latter argument was based on their RV differences. Our data show that the mean RV for the deep photospheric layers (which is close to the value for the star itself) is the same for both stars within the measurement accuracy, $+10 \pm 2 \text{ km s}^{-1}$. The RVs derived from the DIBs and the velocity for the whole complex (M17–Ser OB1) are close to this value. This suggests that both stars belong to this complex (Chentsov & Luud 1989).

The hydrogen line profiles, obtained in 1997, 1998, and 1999, are shown as relationships r vs. RV in Fig. 4. Similar profiles were also observed in 1995 (Nota et al. 1996). The position of the red wing of the $\text{H}\alpha$ emission component varies a little with time. The averaged part of the profile for $\text{RV} \geq 100 \text{ km s}^{-1}$, mirrored with respect to the star’s mean RV, is shown by a dotted line in Fig. 4. It is seen that a significant part of the emission component is hidden by the strong and variable wind absorption. Are we dealing with moving DACs as mentioned in Sect. 1? Fig. 4 does not contradict this suggestion, but the question remains open as HD 168625 is not observed frequently enough.

4.3. HD 183143

The pulsations and RV gradients in the atmosphere of HD 183143 are almost the same as in HD 168625, but the wind absorption components of the hydrogen lines are significantly weaker. This can be clearly seen comparing Fig. 4 and 5. The hydrogen line profiles, obtained in May–August 1997 by G. A. Galazutdinov and F. A. Musaeu with a coude spectrometer of the 1-m telescope of the SAO, are shown in Fig. 5. The parts of the profiles that are not affected by absorption, permit us to estimate the star’s RV. Their centre, marked by a dashed line in Fig. 5, corresponds to $+15 \text{ km s}^{-1}$. This value is close to that obtained for the stationary emissions of Fe II in the near-IR region. It fits with the range of the RVs, we derived for the weakest absorptions ($9\text{--}18 \text{ km s}^{-1}$). The blue parts of the hydrogen profiles in Fig. 5 apparently reflect other phases of the absorption component motion within RVs from -10 to -110 km s^{-1} . However, to prove the existence of these motions, more frequent (perhaps weekly) observations are needed.

4.4. AS 314

The spectral features of AS 314 have been described by Miroshnichenko, Chentsov, & Klochkova (2000). As seen in Fig. 1 and Table 3, the pure emission and P Cyg-type profiles have the same lines as those in the spectrum of HD 168607. However, the P Cyg-type profile shape in AS 314 is simpler: the absorption components are not split and occur at lower velocities (we found the RV variations did not exceed 20 km s^{-1}). Additionally, in contrast to HD 168607, both a positive emission shift and a negative absorption shift increase as the line becomes stronger (Fig. 2b). Nevertheless, some absorption profiles of moderate intensity are more complex. For example, the Cr II(30) lines look split into 2 components like those in spectroscopic binaries with 2 visible spectra. The components’ depths and intensity ratio change with time (Fig. 6). However, the profiles’ total widths remain the same, while the RVs of the red and blue components remain close to those of the single (not split) absorptions of the He I and others group and of the P Cyg-type absorptions of the weak Fe II lines of low excitation, respectively. Therefore, even if AS 314 is a binary system, its components would hardly have close luminosities and spectral types. As one can see in Fig. 6, the form of the Cr II(30) line profiles can be explained by the presence of emission components which do not rise above the continuum, in contrast to the Fe II lines. RVs of these “splitting” (emission) components coincide with those of the purely emission Fe II lines and of the emission components of the P Cyg-type profiles within the measurement errors (Fig. 6). As in HD 168607, these emission components are the least variable: their mean RVs change between -50 and -60 km s^{-1} in the 5 spectra we obtained in 1997–2001. Probably the star’s RV is bound within this interval. However, such a RV is very unusual for the corresponding line of sight in the Milky

Way. We mentioned above that the RV of HD 168607 and HD 168625, which are located in just 4 degrees on galactic longitude from AS 314, is $+10 \text{ km s}^{-1}$. Moreover, among all our objects AS 314 has the largest galactic latitude. Perhaps we are dealing with a runaway star (see Miroshnichenko et al. 2000). We should also note a strong similarity of the spectra of AS 314 and LS 3591, which is probably a low-mass post-AGB star (Venn et al. 1998). Hence, the nature and evolutionary state of AS 314 still need to be studied further.

4.5. HD 160529

The spectroscopic features of HD 160529 have been described by Wolf, Campusano, & Sterken (1974) and Sterken et al. (1991). The former paper was based on spectra obtained in early 1970's, when the star was in a maximum brightness state and had a spectral type A2/3. The latter paper was based on spectra obtained in 1986 (the star was close to the brightness minimum) and in 1990 (brightness minimum, spectral type B8). Our spectrum suggests a spectral type of $A2 \pm 1$ with the line profiles very close to those detected by Wolf et al. (1974). Emission components are seen in the hydrogen lines and in the strongest Fe II lines (not presented in Table 3 and Fig. 7). They are shifted to the red by strong absorption components. Their RVs do not decrease with the line weakening, as in the case of HD 168607 and AS 314, but instead become larger (2 km s^{-1} for H I and $\sim 15 \text{ km s}^{-1}$ for Fe II) and cannot be attributed to the star.

Profiles of the weak absorptions of He I, Si II (represented in Fig. 7 by the He I 5876 Å line) and Fe II of a high excitation (5387 Å in Fig. 7) are single-peaked and almost symmetric. An asymmetry due to a deepening of the red wing appears in stronger absorptions of N I(3) and Si II(2) (6347 Å in Fig. 7). Their RVs were measured using the line cores. The shallow slope of the filled circles (corresponding to the absorptions) sequence in Fig. 2c is due to the fact that most of the Fe II lines with $r \gtrsim 0.85$ have a high excitation. They are shifted blueward with respect to the other absorptions (Table 2).

In profiles of the low excitation Fe II lines one can distinguish at least three components: main, blueshifted with respect to the He I and others, and 2 weaker ones at both wings. The latter are clearly recognizable and suitable for measurements in lines of a moderate intensity. However as the line strengthens, the blue component becomes deeper, while the red one becomes flatter and occupies that part of the profile where the intensity gradient is the largest. As a result, the profile's gravity centre is shifted to the blue. This is seen when comparing the 5363 and 5018 Å Fe II lines in Fig. 7. After Sterken et al. (1991), we believe that the closest RV to that of the star's mass centre (systemic velocity) is the RV, determined for the red components of the split Fe II lines (our value is -14 km s^{-1}). Only these lines can be considered photospheric. Others have to be attributed to the wind base and its higher layers.

5. Summary

In the present atlas we compared spectra of B6–A2 stars of very high luminosities. The spectral features were carefully found and identified in the range 4800–6700 Å. So far only an atlas of one star from our list, HD 183143 has been published (Jenniskens & Desert 1994; Galazutdinov et al. 2000), while only small sections of the spectra of the other objects have been presented in different papers.

Since all the stars are variable (especially LBV candidates), our atlas is valuable as it presents their spectra at certain epochs. Additionally we found some new features of the objects. In particular, our spectra suggest that HD 168625 (B5.7 Ia–0) and HD 183143 (B7.8 Ia) can be considered as objects, showing “blueward migrating DACs” (e.g., Markova 2000). We also suggest a new explanation for the complicated shape of the absorption line profiles in the spectrum of AS 314. Apparently their splitting is due to superposition of narrow emission peaks, which are formed in the extended envelope of the star.

6. Acknowledgments

This work became possible thanks to support by the U.S. Civilian Research & Development Foundation (CRDF) grant, RP1–2264.

References

- Chentsov, E.L., & Luud, L.S. 1989, *Astrofizika*, 31, 5
- Chentsov, E.L. 1995, *Ap&SS*, 232, 217
- Chentsov, E.L., Musaev, F.A., & Galazutdinov, G.A. 1996, *Bull. Spec. Astrophys. Obs.*, 39, 101
- Chentsov, E.L., & Musaev, F.A. 1996, *Astronomy Letters*, 22, 589
- Fullerton, A.W., Gies, D.R., & Bolton, C.T. 1992, *ApJ*, 390, 650
- Galazutdinov, G.A. 1992, *Prepr. of the Spec. Astrophys. Observ.*, No 92
- Galazutdinov, G.A., Musaev, F.A., Krelowski, J., & Walker, G.A.H. 2000, *PASP*, 112, 648
- van Genderen, A.M. 2001, *A&A*, 366, 508
- de Groot, M. 1969, *Bull. Astron. Inst. Netherlands.*, 20, 225
- Humphreys, R.M., & Davidson, K. 1994, *PASP*, 106, 1025
- Hutsemekers, D., Van Drom, E., Gosset, E., & Melnick, J. 1994, *A&A*, 290, 906
- Jenniskens, P., & Desert, F.-X. 1994, *A&AS*, 106, 39
- Johansson, S. 1978, *Phys. Scripta*, 18, 217
- Kaufer, A., Stahl, O., Wolf, B., et al. 1996, *A&A*, 305, 887
- Markova, N. 1986, *A&A*, 163, L3
- Markova, N. 2000, *A&AS*, 144, 391
- Miroshnichenko, A.S., Chentsov, E.L., & Klochkova, V.G. 2000, *A&AS*, 147, 5
- Nota, A., Pasquali, A., Clampin, M., Pollacco, D., Scideri, S., & Livio, M. 1996, *ApJ*, 473, 946
- Panchuk, V.E., Klochkova, V.G., Najdenov, I.D., Vitrichenko, E.A., Vikuljev, N.A., & Romanenko, V.P. 1999, *Prepr. Spec. Astrophys. Observ.* No 139
- Panchuk, V.E., Najdenov, I.D., Klochkova, V.G., Yermakov, S.V., Ivanchuk, A.V., & Murzin, V.A. 1998, *Bull. Spec. Astrophys. Observ.*, 44, 127

- Rivinius, Th., Stahl, O., Wolf, B., et al. 1997, A&A, 318, 819
Robberto, M. & Herbst, T.M. 1998, ApJ, 498, 400
Sterken, C., Gosset, E., Juettner, A., Stahl, O., Wolf, B., &
Axer, M. 1991, A&A, 247, 383
Striganov, A.R., & Odintsova, G.A. 1982, Tables of spectral
lines of atoms and ions, Moscow, Energoizdat
van Genderen, A.M., van den Bosch, F.C., Dessing, F., et al.
1992, A&A, 264, 88
Venn, K., Smartt, S.J., Lennon, D.J., & Dufton, P.L. 1998,
A&A, 334, 987
Wolf, B., Campusano, L., & Sterken, C. 1974, A&A, 36, 87

List of Objects

- 'HD 168625' on page 1
'HD 160529' on page 1
'HD 168607' on page 1
'AS 314' on page 1
'HD 183143' on page 1
'LS 3591' on page 5

Table 3. Line identification and intensities in the spectra of LBV studied

Line (Mult)	λ_{lab}	HD168625	HD183143	HD168607	AS314	HD160529
1	2	3	4	5	6	7
TiII (92)	4779.98					0.84
DIB	80.04	0.96	0.96	0.95		
NII (20)	88.13	0.98	0.99			
TiII (17)	98.54					0.96
NII (20)	4803.29	0.97	0.98			
TiII (92)	05.09					0.77
CrII (30)	12.35					0.88
SII (9)	15.55	0.94	0.94	0.95	0.94	
CrII (30)	24.14			0.98	0.86	0.66
FeII (30)	33.21					0.98
CrII (30)	36.22				0.99	0.87
CrII (30)	48.25			0.99	0.90	0.72
MgII (24)	51.08				0.97	0.97
CrII (30)	56.19				0.98	0.72
H β	61.33	0.70	0.70	0.3/4.0	0.2/3.0	0.4/1.4
CrII (30)	64.32				0.93	0.75
FeII (25)	71.27					0.92
TiII (114)	74.03					0.86
CrII (30)	76.40				0.93	0.72
CrII (30)	84.60				0.98	0.88
CrII (36)	91.55					0.94
FeII (36)	93.78					0.96
CrII (190)	4901.65				0.99	0.95
FeII	08.15					0.97
TiII (114)	11.19					0.82
FeII	13.30				0.96	0.94
SII (15)	17.21	0.96	0.96	0.97	0.97	
FeI (318)	20.50					0.94
HeI (48)	21.93	0.73	0.75			
FeII (42)	23.92	0.90	0.87	0.61/1.15	0.32/1.3	0.35/1.11
BaII (1)	34.09					0.96
FeII	48.80				0.96	0.92
FeII	51.59			0.99	0.93	0.94
FeI (318)	57.58					0.90
DIB	63.90	0.97	0.97	0.95	0.96	0.98
OI (14)	68.0:				0.98	0.98
FeII	77.03				0.96	0.96
FeII	84.50				0.94	0.92
DIB	84.81	0.99	0.99	0.99		
NII (24)	87.37	0.99	0.99			
FeII	90.50				0.95	0.91
SII (7)	91.97	0.97	0.96			
FeII (36)	93.35			0.97	0.93	0.90
NII (24)	94.36	0.98	0.98			
NII (19)	5001.3:	0.94	0.94			
FeII	01.92			0.95	0.83	0.82

continued on the next page

<i>continued from previous page</i>						
1	2	3	4	5	6	7
FeII	04.20			0.99	0.87	0.88
NII (19,6)	05.15	0.96	0.97	0.98		
FeII	06.84					0.97
NII(24)	07.33	0.98	0.09	0.99		
FeII	07.7:				0.94	0.94
SII (7)	09.56	0.97	0.97	0.97	0.98	
TiII (113)	10.2:					0.94
TiII (113)	5013.4:					0.95
SII (7)	14.07	0.98	0.97	0.97	0.96	
HeI (4)	15.68	0.80	0.83	0.85	0.90	
FeII (42)	18.44	0.92	0.87	0.57/1.15	0.29/1.4	0.32/1.17
FeII	22.79				0.94	0.94
FeII	26.80				0.97	0.97
SII (1)	27.22	0.97	0.98	0.98		
FeII	30.64				0.92	0.81
SII (7)	32.45	0.93	0.92	0.92		
FeII	32.71				0.89	0.91
FeII	35.71			0.98	0.86	0.83
SiII (5)	41.03	0.95	0.93	0.94	0.75	0.71
NII (4)	45.10	0.96	0.97	0.98		
FeII	47.64				0.92	0.93
HeI (47)	47.74	0.91	0.92	0.94		
SiII (5)	56.06	0.90	0.88	0.89	0.68	0.65
FeII	61.73			0.99	0.93	0.92
FeII	67.89				0.97	0.97
FeII	70.90				0.93	0.94
TiII (113)	72.29					0.97
FeIII(5)	73.90	0.98	0.98			
FeII	74.05				0.96	0.97
FeII	75.77				0.95	0.96
FeII	82.23				0.96	0.97
FeIII(5)	86.72	0.97	0.98			
FeII	87.26				0.96	0.94
FeII	89.22				0.96	0.96
FeII	93.56				0.94	0.93
FeII	97.27				0.95	0.93
FeII(35,185)	5100.74		0.98	0.97	0.92	0.86
SII (7)	03.34	0.98	0.98	0.98	0.97	
FeII	06.11				0.98	0.97
FeII	17.03				0.98	0.98
FeII	23.19					0.97
FeIII(5)	27.35	0.95	0.95			
FeII (167)	27.85				0.95	
TiII (86)	29.15					0.86
FeII (35)	36.79					0.98
FeII	44.36				0.94	0.92
FeII	49.45				0.91	0.89
FeII	52.9:				0.98	
TiII (70)	54.06					0.83
FeIII(5)	56.12	0.95	0.96			

continued on the next page

<i>continued from previous page</i>						
1	2	3	4	5	6	7
FeII	57.6:				0.97	0.98
FeII (167)	60.85					0.91
FeII (42)	69.03	0.92	0.83	0.52/1.15	0.22/1.47	0.28/1.22
MgI (2)	72.69				0.96	0.80
FeII	77.3:				0.94	0.96
MgI (2)	83.61				0.96	0.82
TiII (86)	85.90					0.87
TiII (70)	88.68					0.81
FeII (49)	97.58		0.98	0.95/1.12	0.82/1.07	0.69
FeII	99.12				0.98	0.97
FeII	5200.81				0.96	0.98
SII (39)	01.1:	0.98	0.98	0.99		
FeII	03.64				0.97	0.96
CrII (24)	10.87				0.98	0.94
SII (39)	12.62	0.97	0.97	0.98	0.97	
FeII	15.5:				0.96	0.94
FeII	16.85			0.98	0.89	0.88
FeII	18.84				0.97	0.96
TiII (70)	26.53				0.96	0.82
SII (1)	27.22	0.99	0.98	0.98		
FeII	27.49				0.86	0.80
FeII (49)	34.62		0.98	0.92/1.12	0.82/1.10	0.64
FeIII(113)	35.66	0.97	0.98			
CrII (43)	37.32				0.97	0.78
FeIII(113)	43.31	0.99				
CrII (23)	46.77				0.96	0.95
FeII	47.95				0.92	0.92
FeII	51.23			0.99	0.91	0.91
FeII (49)	54.93			0.99/1.03	0.94/1.11	0.87
FeII	60.26	0.99	0.96	0.96	0.80	0.84
FeII (48)	64.80			0.99/1.02	0.86/1.02	0.82
FeII (185)	72.40				0.97	0.94
FeII (49)	76.00	0.98	0.96	0.88/1.08	0.72/1.06	0.52/1.07
CrII (43)	80.08					0.87
FeII (41)	84.10			1.07	0.95/1.15	0.81
FeII	91.67			0.99	0.92	0.89
MnII (11)	99.28				0.97	0.97
MnII (11)	5302.32				0.98	0.97
CrII (24)	05.85					0.93
CrII (43)	08.44					0.94
CrII (43)	10.70					0.95
CrII (43)	13.58				0.98	0.88
FeII (49,48)	16.65	0.98	0.93	0.83/1.15	0.70/1.20	0.55/1.02
SII (38)	20.73	0.96	0.95	0.96	0.96	
FeII (49)	25.56			0.99/1.03	0.97/1.07	0.87
OI (12)	29.5:				0.96	0.94
OI (12)	30.74				0.94	0.95
CrII (43)	34.87				0.98	0.88
TiII (69)	36.79					0.90
FeII (48)	37.73					0.88

continued on the next page

<i>continued from previous page</i>						
1	2	3	4	5	6	7
FeII	39.59			0.98	0.92	0.91
SII (38)	45.72	0.97	0.97	0.97	0.97	
CrII (24,23)	46.4:					0.94
FeII (48)	62.86			0.97/1.08	0.92/1.18	0.75
DIB	63.60	0.97	0.97	0.97		
FeII	70.30				0.98	0.97
TiII (69)	81.02					0.92
FeII	87.07				0.92	0.91
FeII	95.86				0.94	0.91
FeII	5402.06		0.99	0.99	0.89	0.88
DIB	04.50	0.96	0.96	0.95	0.96	0.94
CrII	07.61					0.97
FeII (184)	08.81				1.03	0.97
FeII (48)	5414.06				0.99/1.07	0.95
FeII	14.85				0.98	0.96
TiII (69)	18.80					0.96
DIB	18.90	0.99	0.99	0.98		
CrII (23)	20.90					0.97
FeII (49)	25.25			0.99/1.05	0.97/1.10	0.87
FeII	27.82			1.04	1.12	0.98
SII (6)	28.67	0.95	0.96	0.96	0.97	
FeII	29.99			0.99	0.93	0.91
SII (6)	32.82	0.92	0.92	0.93	0.96	0.93
OI (11)	35.5:			0.99	0.97	0.97
FeII	45.80				0.98	0.97
SII (6)	53.83	0.88	0.87	0.88	0.90	0.95
CrII (50)	55.80					0.96
FeII	57.72				0.97	0.97
FeII	65.93				0.90	0.90
FeII	66.92			0.99/1.03	0.96	0.95
SII (6)	73.62	0.95	0.94	0.95	0.95	0.96
FeII	75.83				0.98	0.98
CrII (50)	78.37					0.92
FeII	82.31				0.91	0.92
DIB	87.6:	0.97	0.96	0.96		
FeII	87.63				0.93	0.92
FeII	92.5:				0.94	0.93
DIB	94.10	0.95	0.95	0.94		
FeII	94.63				0.95	0.93
CrII (50)	5502.07					0.96
FeII	02.68				0.96	0.91
CrII (50)	03.20					0.96
FeII	06.20	0.98	0.97	0.95	0.86	0.86
DIB	08.35	0.97	0.97	0.97		
CrII (50)	08.61				0.98	0.96
SII (6)	09.72	0.96	0.94	0.94		
CrII (23)	10.71				0.93	0.93
DIB	12.64	0.98	0.98	0.96		
OI (25)	12.7:				0.98	0.98
FeII (56)	25.12				1.04	0.96

continued on the next page

<i>continued from previous page</i>						
1	2	3	4	5	6	7
ScII (31)	26.81					0.87
FeII	29.06					0.93
FeII (224)	29.93			1.03	0.98/1.07	
FeII	32.09				0.98	0.96
FeII (55)	34.84	0.97	0.97	0.98/1.06	0.92/1.18	0.79
DIB	41.62	0.99	0.99	0.98		
FeII (166)	44.76				0.94	0.93
DIB	44.96	0.96	0.97	0.96		
FeII	48.21				0.99	0.98
FeII	49.00				0.98	0.97
OI (24)	55.0:				0.99	
SII (6)	56.01	0.99	0.99	0.99		
SII (6)	64.98	0.97	0.97	0.97	0.97	
FeII	67.84			1.03	1.07	
[OI] 3F	77.34					
SII (11)	78.89	0.98	0.98	0.98		
FeII	5587.08			1.02	1.07	0.98
FeII	88.23				0.96	0.96
AlII (16)	93.30			1.03		
SII (11)	5606.15	0.96	0.95	0.95	0.96	0.98
DIB	09.73	0.98	0.98	0.98		0.99
SII (11)	16.64	0.99	0.98	0.98	0.98	0.98
SII (14,11)	40.1:	0.90	0.89	0.89	0.90	0.93
FeII	45.40			0.98	0.95	0.95
SII (14)	47.03	0.95	0.95	0.94	0.94	0.98
FeII	48.90				0.98	0.99
ScII (29)	57.87					0.89
FeII (57)	57.92				0.99/1.06	
SII	59.99	0.97	0.97	0.97	0.97	0.98
SII	64.78	0.98	0.98	0.98	0.98	
NII (3)	66.63	0.95	0.97	0.98		
SiII	69.56			0.99	0.98	0.98
NII (3)	76.02	0.96	0.97	0.98		
NII (3)	79.56	0.91	0.94	0.96	0.99	
NaI (6)	82.63					0.96
ScII (29)	84.18					0.97
NII (3)	86.21	0.98	0.99			
NaI (6)	88.20				0.98	0.92
FeII	91.00				0.98	0.97
AlIII(2)	96.60	0.93	0.95	0.97	0.99	
DIB	5705.20	0.94	0.94	0.94	0.98	0.96
NII (3)	10.77	0.95	0.96	0.96		
DIB	19.30	0.97	0.97	0.97		
AlIII(2)	22.73	0.96	0.97	0.98	0.99	
SiIII(4)	39.73	0.96	0.97	0.98		
FeII (164)	47.90				0.98	0.97
DIB	66.16	0.97	0.97	0.96	0.98	0.98
DIB	69.05	0.99	0.99	0.98		
DIB	72.60	0.95	0.95	0.95	0.99	0.98
DIB	75.78	0.95	0.95	0.95	0.99	0.97

continued on the next page

<i>continued from previous page</i>						
1	2	3	4	5	6	7
DIB	80.37	0.66	0.65	0.63	0.86	0.71
DIB	85.05	0.98	0.99	0.99		
DIB	89.06	0.96	0.96	0.97	0.99	0.98
DIB	93.22	0.97	0.97	0.97	0.99	0.98
DIB	96.96	0.80	0.80	0.76	0.86	0.83
SiII (8)	5800.47	0.99	0.99	0.99	0.98	
SiII (8)	06.74	0.99	0.98	0.98	0.97	0.98
DIB	09.24	0.98	0.98	0.98		0.99
DIB	11.96	0.99	0.99	0.99		
FeII	13.7:				0.98	0.98
DIB	18.75	0.99	0.99	0.99		
DIB	28.46	0.98	0.98	0.98		
FeIII(114)	33.93	0.98	0.99	0.99		
FeII	42.30				0.98	0.98
DIB	44.2:	0.97	0.97	0.98		0.98
DIB	49.80	0.91	0.91	0.89	0.95	0.95
NeI (6)	52.49	0.99	0.98	0.98	0.98	
SiII (8)	68.40	0.99	0.98	0.98	0.97	
FeII	71.77			0.99	0.97	0.97
HeI (11)	5875.72	0.61	0.67	0.75	0.83	0.90
NaI (1)	89.95	0.12	0.06	0.14	0.22	0.06
NaI (1)	95.92	0.15	0.10	0.16	0.26	0.07
SiII (4)	5957.56			0.97	0.89	0.89
FeII	61.71				0.93	0.93
FeII	65.63				0.97	0.96
SiII (4)	78.93	0.98	0.96	0.98	0.82	0.84
FeII (46)	91.37				0.98/1.15	0.95
DIB	99.63	0.98	0.99	0.98		
DIB	6005.03	0.98	0.98	0.98		
DIB	10.65	0.96	0.95	0.96		0.97
DIB	19.36	0.98	0.98	0.98		0.98
DIB	27.48	0.98	0.98	0.98		0.99
DIB	37.61	0.98	0.98	0.98		0.99
P II (5)	43.12	0.99	0.98	0.98	0.98	
FeII (200)	45.46				0.97	0.98
OI (22)	46.4:				0.97	
CrII (105)	53.46					0.99
DIB	59.67	0.99	0.99	0.99		0.99
FeII	60.99			1.02	1.02	0.99
DIB	65.20	0.97	0.98	0.98		
NeI (3)	74.34	0.99	0.98	0.98	0.99	
FeII (46)	84.10			1.03	0.98/1.10	0.96/1.03
DIB	89.78	0.95	0.96	0.95		0.98
NeI (3)	96.16	0.97	0.97	0.97	0.97	0.98
FeII (200)	6103.54				1.02	0.98
DIB	08.05	0.98	0.98	0.98		0.99
DIB	13.20	0.97	0.97	0.97		
FeII (46)	13.33				0.99/1.05	0.98
DIB	16.80	0.98	0.98	0.98		
MnII (13)	26.0:					0.97

continued on the next page

<i>continued from previous page</i>						
1	2	3	4	5	6	7
MnII (13)	29.0:					0.97
DIB	39.94	0.97	0.97	0.97		
NeI (1)	43.06	0.96	0.96	0.96	0.96	
FeII (74)	47.74			0.99/1.03	0.95/1.10	0.88
FeII (74)	49.25			1.04	1.08	0.86
OI (10)	56.3:	0.98	0.97	0.95	0.86	0.92
OI (10)	58.18	0.98	0.97	0.95	0.85	0.92
DIB	61.93	0.98	0.98	0.98		
NeI (5)	63.59	0.98	0.98	0.98	0.98	
unident.	73.0:			1.03	1.05	
FeII (200)	75.15				0.98/1.03	0.97
FeII (163)	79.39				0.98/1.03	0.97
DIB	94.73	0.98	0.99	0.99		
DIB	95.96	0.89	0.89	0.89	0.95	0.92
DIB	6203.08	0.87	0.87	0.87	0.95	0.90
DIB	11.67	0.98	0.98	0.98		0.99
DIB	15.79	0.99	0.99	0.99		
DIB	23.56	0.99	0.99	0.99		
AlII (10)	31.75			1.03		0.99
FeII	33.53			1.02	1.03	0.98
DIB	34.03	0.97	0.98	0.98		
DIB	36.67	0.99	0.99			
FeII (74)	6238.39	0.99	0.99	0.99/1.05	0.89/1.13	0.87
FeII (74)	39.91	0.99	0.99	1.07	1.05	0.90
AlII (10)	43.36			1.04	0.99	0.97
FeII (74)	47.55	0.99	0.98	0.98/1.07	0.80/1.14	0.80
FeII	48.89			1.08	1.06	0.95
DIB	50.84	0.99	0.99			
NeI (5)	66.50	0.97	0.97	0.97	0.98	
DIB	69.75	0.88	0.87	0.90	0.97	0.94
DIB	83.85	0.66	0.66	0.65	0.89	0.70
FeII	6317.99			1.15	1.13	0.87
DIB	24.80	0.98	0.98	0.98		0.98
DIB	29.97	0.98	0.98	0.98		
FeII (199)	31.95				1.03	0.97
NeI (1)	34.43	0.99	0.98	0.98	0.98	
SiII (2)	47.10	0.77	0.68	0.59	0.57	0.53
DIB	53.34	0.99	0.98	0.98		
DIB	62.30	0.98	0.98	0.99		0.98
DIB	67.25	0.97	0.97	0.97		0.98
FeII (40)	69.46				0.98/1.08	0.97
SiII (2)	71.36	0.80	0.71	0.64	0.62	0.57
DIB	75.95	0.92	0.94	0.92	0.97	0.95
DIB	79.29	0.81	0.85	0.80	0.89	0.91
NeI (3)	82.99	0.98	0.98			
FeII	83.72			1.09	1.09	0.94
FeII	85.46			1.06	1.07	0.98
DIB	97.39	0.96	0.98	0.96	0.97	0.97
NeI (1)	6402.25	0.92	0.91	0.92	0.93	0.97
FeII (74)	07.25				0.99/1.05	

continued on the next page

<i>continued from previous page</i>						
1	2	3	4	5	6	7
DIB	10.18	0.99	0.99	0.99		
DIB	13.93	0.99	0.99	0.99		
FeII (74)	16.92			0.99/1.04	0.90/1.16	0.90
DIB	25.70	0.96	0.96	0.98	0.98	0.98
FeII (40)	32.68	0.99	0.99	0.99/1.05	0.96/1.22	0.93/1.07
DIB	39.50	0.97	0.97	0.95		
FeII	42.95			1.04	1.05	0.97
DIB	45.20	0.93	0.93	0.92	0.97	0.95
DIB	49.14	0.97	0.98	0.98		
OI (9)	53.60				0.98	0.98
FeII (74)	56.38	0.96	0.96	0.97/1.05	0.77/1.20	0.75
NII (8)	82.05	0.97	0.98			
NI (21)	82.70				0.98	0.90
NeI (3)	6506.53	0.97	0.96	0.97		
FeII (40)	16.08				0.97/1.17	
DIB	20.56	0.98	0.98			
MgII (23)	45.97				0.97	0.92
H α	62.81	1.65	1.75	0.30/6.1	0.15/9.5	0.20/4.0
CII (2)	78.05	0.82	0.85	0.88	0.93	
CII (2)	82.88	0.86	0.90	0.90	0.94	
FeII	86.70					0.98
DIB	97.31	0.98	0.97	0.98		
NeI (6)	98.95	0.97	0.97	0.98		
FeII	6600.03					0.97
NII (31)	6610.57	0.99	0.99	0.99		
DIB	13.56	0.67	0.72	0.70	0.87	0.81
NI (20)	22.54					0.99
FeII (210)	27.24				0.98/1.03	0.98
NI (20)	44.96					0.96
NI (20)	53.46					0.98
DIB	60.64	0.91	0.91	0.92	0.94	0.96
SiII	71.88	0.95	0.95	0.95	0.96	0.98
HeI (46)	78.15	0.64	0.71	0.78	0.88	0.93
DIB	89.30	0.98	0.99	0.98		
DIB	94.48	0.98	0.99			
DIB	99.24	0.93	0.94	0.94	0.97	0.97
DIB	6701.98	0.97	0.97	0.98	0.99	0.99

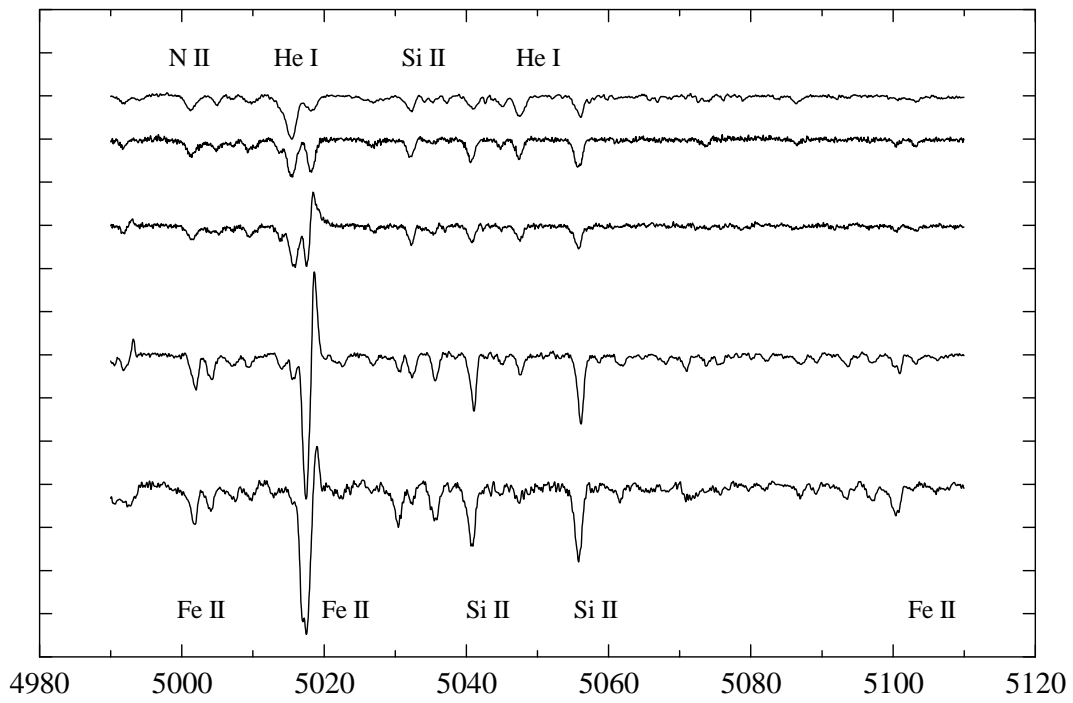


Fig. 1. An example page of the spectral atlas.

The spectra are shown in the following order from top bottom: HD 168625, HD 183143, HD 168607, AS 314, and HD 160529. The intensities (ordinates) are in continuum units with tick mark intervals of 0.2. The wavelengths (abscissas) are in Å.

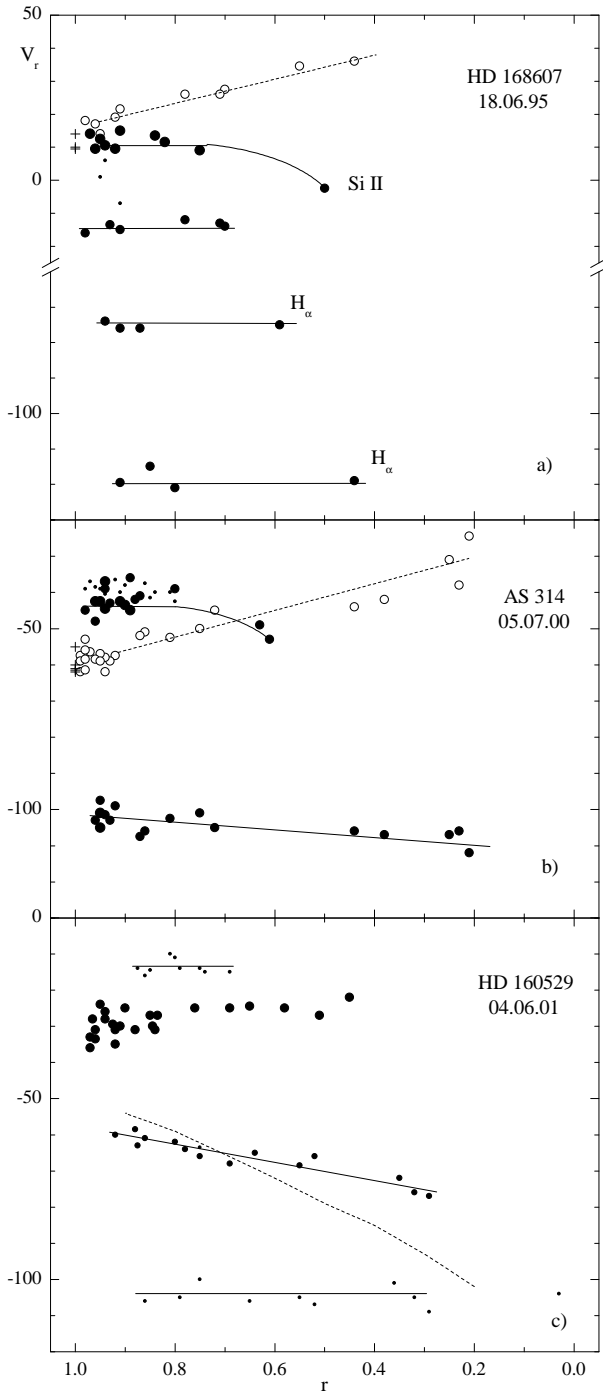


Fig. 2. Relationships between the RVs and central residual intensities of the absorption lines and absorption components of P Cyg-type profiles in the spectra of HD 168607 (panel a), AS 314 (panel b), and HD 160529 (panel c). Each symbol represents a separate line or component. In panels (a) and (b) large filled circles represent pure absorption lines, small filled circles - high-excitation absorption lines of Fe II, open circles - lines with emission components, and pluses - Fe II lines with stationary emissions. In panel (c) large filled circles represent lines of He I, Si II, and high-excitation Fe II lines; small filled circles and dots represent main and secondary components of low-excitation Fe II lines. The lines show linear fits to the relationships. The dashed line in panel (c) shows the dependence of RVs of the whole profile gravity centre from the relative intensities of the latter group of lines.

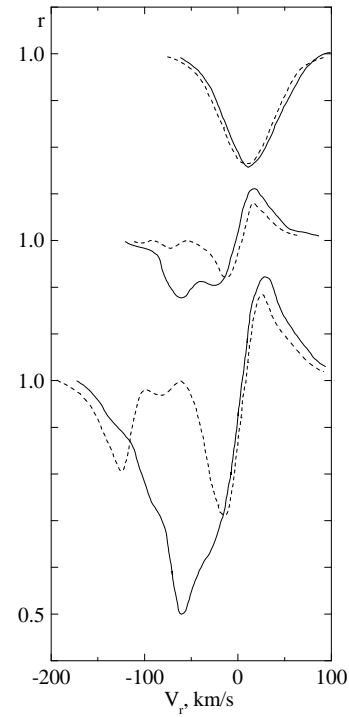


Fig. 3. Line profiles in the spectra of HD 168607 obtained on 1992 August 14 (solid lines) and on 1995 June 18 (dashed lines). From top bottom: He I(11) 5876 Å, Fe II(49) 5276 Å, Fe II (42) 5169 Å.

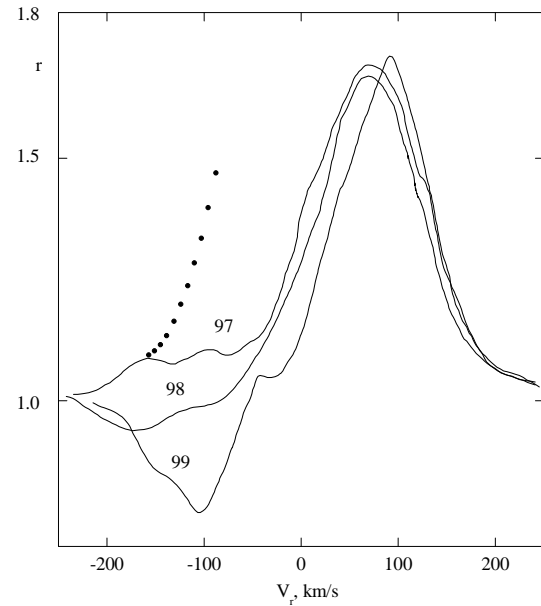


Fig. 4. The Balmer line profiles in the spectra of HD 168625 obtained on 1997 July 23, 1998 June 19 and 1999 June 4. The dots represent the blue wing position with the absence of the absorption component. The dotted line was derived from the line symmetry assumption (see text).

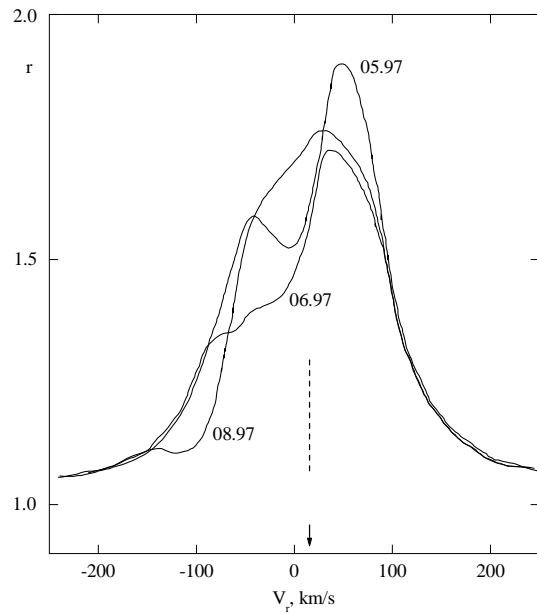


Fig. 5. The $H\alpha$ line profile in the spectra of HD 183143 obtained on 1997 May 14, 1997 June 6 and 1997 August 20. The dashed line marks the centre of the symmetric part of the profiles.

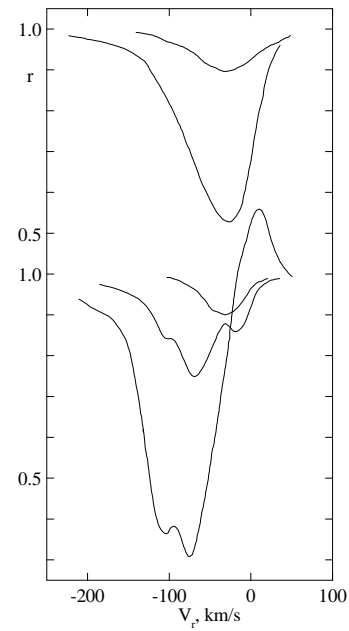


Fig. 7. Line profiles in the 2001 June 4 spectrum of HD 160529. From top bottom: He I(11) 5876 Å, Si II(30) 6347 Å, Fe II 5387 Å, Fe II(48) 5363 Å, Fe II(42) 5018 Å.

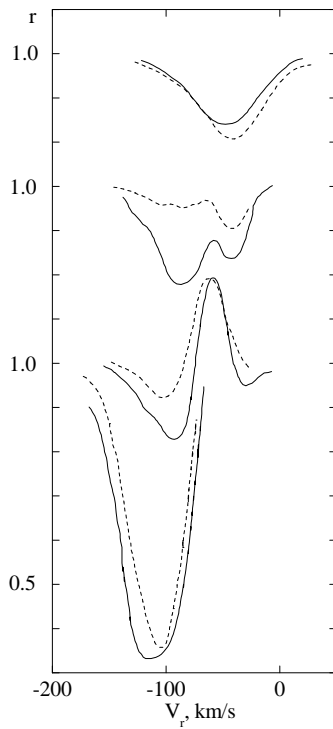


Fig. 6. Line profiles in the spectra of AS 314 obtained on 2000 July 5 (dashed lines) and on 2001 June 4 (solid lines). From top bottom: He I(11) 5876 Å, Cr II(30) 4824 Å, Fe II(48) 5363 Å, Fe II(42) 5169 Å (absorption part only).